Title
Structural Stability and Binding Strength of a Designed Peptide–Carbon Nanotube Hybrid

Journal
The Journal of Physical Chemistry C, 117(49)

ISSN
1932-7447

Authors
Roxbury, Daniel
Zhang, Shao-Qing
Mittal, Jeetain
et al.

Publication Date
2013-12-12

DOI
10.1021/jp405618p

Peer reviewed

Published in final edited form as:
J Phys Chem C Nanomater Interfaces. 2013 December 12; 117(49): 26255–26261. doi:10.1021/jp405618p.

Structural Stability and Binding Strength of a Designed Peptide-Carbon Nanotube Hybrid

Daniel Roxbury[1], **Shao-Qing Zhang**[3,4], **Jeetain Mittal**[1], **William F. DeGrado**[3], and **Anand Jagota**[1,2,*]

[1]Department of Chemical Engineering

[2]Bioengineering Program, Lehigh University

[3]Department of Physics and Astronomy, University of Pennsylvania

[4]Department of Pharmaceutical Chemistry, University of California, San Francisco

Abstract

Biological polymers hybridized with single-walled carbon nanotubes (SWCNTs) have elicited much interest recently for applications in SWCNT-based sorting as well as biomedical imaging, sensing, and drug delivery. Recently, de novo designed peptides forming a coiled-coil structure have been engineered to selectively disperse SWCNT of a certain diameter. Here we report on a study of the binding strength and structural stability of the hybrid between such a “HexCoil-Ala” peptide and the (6,5)-SWCNT. Using the competitive binding of a surfactant, we find that affinity strength of the peptide ranks in comparison to that of two single-stranded DNA sequences as $(GT)_{30}$-DNA > HexCoil-Ala > $(TAT)_4T$-DNA. Further, using replica exchange molecular dynamics (REMD), we show that the hexamer peptide complex has both similarities with and differences from the original design. While one of two distinct helix-helix interfaces of the original model was largely retained, a second interface showed much greater variability. These conformational differences allowed an aromatic tyrosine residue designed to lie along the solvent-exposed surface of the protein instead to penetrate between the two helices and directly contact the SWCNT. These insights will inform future designs of SWCNT-interacting peptides.

Keywords

SWCNT; Peptide; DNA; Molecular Dynamics; Stability

1. Introduction

Much effort has been expended in recent years studying and developing desirable properties and applications of the single-walled carbon nanotube (SWCNT). These include their ability as strengthening agents for composite materials,[1] construction of field-effect transistor devices,[2–3] and *in vitro/in vivo* imaging and targeted delivery agents in biomedical

[*]*corresponding author*: D331 Iacocca Hall, Lehigh University, Bethlehem PA 18017 (USA) (1-610 758 4396); anj6@lehigh.edu).

ASSOCIATED CONTENT

Supporting Information.

Additional data on circular dichroism, two-dimensional fluorescence maps, convergence of helicity in simulation, configuration stability and helical interface analysis. This material is available free of charge via the Internet at http://pubs.acs.org.

Author Contributions

The manuscript was written through contributions of all authors. All authors have given approval to the final version of the manuscript.

applications.[4–8] As objects foreign to cells, SWCNTs present a certain degree of cytotoxicity.[9–10] However, this can be reduced greatly by appropriate surface functionalization.[11–13] Additionally, upon production, SWCNTs tend to clump together in bundles of mixed chirality (electronic species) due to their high aspect ratios and hydrophobic surface.[14–15] Numerous methods have been developed to solubilize and sort SWCNTs by length,[16–17] diameter,[18] and electronic structure by hybridization with a dispersant molecule.[19] The dispersant molecule can range from small inorganic surfactants (e.g., sodium dodecyl sulfate)[20] to biological polymers (short DNA oligomers or peptides).[21–23] The ability of certain short strands of DNA to recognize particular SWCNTs from a chirality-diverse mixture, enabling single-species purification, has been demonstrated.[24]

The design of peptides for SWCNT dispersion has also been investigated.[21, 25–26] In general, a peptide with sufficient hydrophobic residues located at appropriate sites along its backbone will be able to disperse a SWCNT in aqueous medium to some extent. By designing peptide sequences to promote the arrangement of hydrophobic residues to one side of an alpha helix, SWCNT dispersion abilities were shown to be significantly increased.[21, 25] More recent studies have attempted to selectively disperse SWCNTs of a particular diameter or chirality from a mixture using designed peptides.[27] Grigoryan et al. have developed a *de novo* peptide design method using sequences known to form α helices that then assemble into hexa-coiled supramolecular structures.[27] By controlling the diameter of the hexa-coiled structure through sequence modulation, they have been able to selectively disperse (6,5) and (8,3)-SWCNTs from mixtures. When design is based on the primary structure, it is implied that the peptide will assume some adsorbed conformation likely different from its solution state. When stable secondary and tertiary structures are designed, as in the example just cited, it is assumed that this structure will unravel by virtue of interaction with the SWCNT, which may or may not be the case.[28]

Here, we study the affinity of a particular 30-amino acid long peptide, “HexCoil-Ala”, for the (6,5)-SWCNT through experimentation and simulation.[27] This alanine-rich sequence has been shown to singly-disperse SWCNTs, as indicated by strong near-infrared (NIR) photoluminescence.[20] We used surfactant-induced displacement of adsorbed molecules from the SWCNT surface to rank and quantify binding strength compared to chosen DNA sequences.[29] Ranking was then confirmed by creating dispersions of raw SWCNTs in mixtures of peptide or DNA, and surfactant. NIR absorbance measurements were used to identify which type of molecule remained on the SWCNT. Using replica exchange molecular dynamics (REMD) simulation, we probed the stability of the hexamer peptide-SWCNT construct. The symmetry of the original hexamer dictated two distinct helix-helix interfaces that were considered in the design process. Simulations showed that only one of the two interfaces remained stable on the 50 ns time scale, and rearrangements were observed in the interaction of the helices, specifically that of an aromatic Tyr residue with the SWCNT due to π–π interactions.

2. Methodologies

As described by Grigoryan et al.,[27] dispersions of HexCoil-Ala peptide were created using Comocat nanotubes (*SWeNT*). First, 1 mg of previously synthesized, purified, and lyophilized HexCoil-Ala (AEAESALEYAQQALEKAQLALQAARQALKA) was added to 0.1 mg of raw nanotubes in a 100 mM phosphate buffer at pH 7.4. The solution was then probesonicated (*Branson*) at 8 Watts for 90 minutes in an ice-cooled bath followed by 6 hours of centrifugation (*Eppendorf*) at 16,000 times the force of gravity. The resultant supernatant was then extracted and unbound peptide was removed with the use of a 100 kDa microcentrifuge spin filter (*Millipore Amicon*). The peptide-SWNCT hybrid was then stored

at 4 °C with no noticeable SWCNT aggregation seen over several months during the course of the study. Additionally, hybrids of DNA sequences $(GT)_{30}$ or $(TAT)_4T$, and Comocat nanotubes, in a weight ratio of 1:1, were also created using the same procedure for comparison with peptide-SWCNT.

Initial absorbance and fluorescence spectra of the peptide-SWCNT dispersion were measured. A UV/Vis/NIR spectrophotometer (*Varian Cary50*) was used to measure the absorbance spectrum from 200–1100 nm of the dispersion in a quartz microcuvette. A prominent NIR peak was observed at 992 nm, indicative of the E_{11} bandgap transition for the (6,5)-SWCNT. Furthermore, a two-dimensional excitation/emission NIR fluorescence map (*Horiba Yvon Jobin Fluorolog-3*) of the peptide-SWCNT dispersion was measured. The excitation and emission ranges were 500–800 nm and 900–1200 nm, respectively, with a slit width of 8 nm and data interval of 3 nm. Again, the dominant peak corresponded to a (6,5)-SWCNT with excitation/emission pair of 569/992 nm.

In accordance with a previously used method,[29] a small-molecule surfactant, sodium dodecylbenzene sulfonate (SDBS), was used in an attempt to displace the peptide off the surface of a (6,5)-SWCNT. A solution of 0.2 wt % SDBS in the same 100 mM phosphate buffer used for SWCNT dispersion was held at 60 °C in the quartz cuvette. In a 1:1 v/v ratio, peptide-SWCNT solution was introduced into the cuvette and pipette-mixed at time zero. The effective SDBS concentration was thus reduced to 0.1 wt %, less than the critical micelle concentration (CMC) of the surfactant.[29] Over the course of the next 30 minutes, the NIR absorbance was scanned from 950–1050 nm at one minute intervals to monitor the progress of the surfactant displacement reaction. The procedure was then repeated using DNA with sequences $(GT)_{30}$ and $(TAT)_4T$-SWCNT. In addition, in place of SDBS, a different surfactant, sodium cholate, was used to attempt surfactant exchange. Displacement by the surfactant causes a solvatochromic shift in the peak of the absorbance spectrum. By tracking this shift the relative progress and speed of the reaction can be monitored.

Binary dispersions (mixtures of SDBS and peptide, or SDBS and $(GT)_{30}$/$(TAT)_4T$, in equal mass ratios) were created. The raw SWCNT sample was then sonicated in the presence of this mixture of molecules (10:10:1 by weight) for 90 minutes and centrifuged as previously described, allowing the surfactant and peptide or DNA to compete for the SWCNT surface. Following this procedure, NIR absorbance spectra of the supernatant were measured.

In addition to changes in the absorbance, a final fluorescence map of the peptide-SWCNT solution was measured after surfactant exchange using the same parameters as described previously. Circular dichroism (CD) in the far-UV (190–240 nm) was measured (*Jasco J-815*) using a quartz cuvette with a path length of 1 mm to investigate characteristics of the secondary structure of the peptide-SWCNT hybrids as they encounter surfactant. The surfactant chosen for this study was sodium dodecyl sulfate (SDS) for its relatively low absorbance in the UV region as compared to SDBS or sodium cholate. The peptide remained at 1 mg/mL with SDS at a concentration of 0.1 % wt.

For the MD study, we began by using the HexCoil-Ala structure available on the RCSB protein data bank (PDB) as structure – 3S0R. This file contains two chains, A and B, in an antiparallel configuration. Three copies of the PDB file were placed around the exterior of the (6,5)-SWCNT in an orientation permitting hydrophobic peptide residues to be in close proximity with the SWCNT surface. The SWCNT was 8.12 nm long with a diameter of 0.75 nm. The length was chosen such that one end of the frozen SWCNT would exactly adjoin its periodic image thus creating an infinitely long SWCNT. SWCNT Carbon atoms were modeled with sp2-hybridization with detailed parameters provided in previous publications.[30–31] The peptide-SWCNT hybrid was then solvated in an 8.12 × 5.00 × 5.00

nm water-box containing approximately 6,200 TIP3P model[32] water molecules with the appropriate number of sodium counter-ions to balance the net-negatively charged peptide (Figure 1b). Periodic boundary conditions were applied in all directions with long-range electrostatic interactions calculated using the particle mesh Ewald method.[33] All structures were visualized in *VMD*.[34]

Replica exchange MD (REMD) accesses a greater fraction of available microstates by overcoming high energy barriers,[35–36] and has been used in the past to determine equilibrium structures in simulations of DNA-SWCNT hybrids.[30–31, 37] Here, the Gromacs 4.5.3 simulation package[38–40] was used in conjunction with the Amber03d[41] protein force field for REMD simulation. This particular protein force field has been successfully used in previous protein folding simulations of proteins containing α-helix and β-sheet structures[42–43]. Forty replicas were simulated in parallel with temperatures ranging from 296 K to 587 K. The replica temperatures were chosen such that exchange acceptance ratios between the replicas remained around 10% with an exchange time of 1 ps. The structure was run for 50 ns of REMD simulation, for a total computation time of 40 × 50 ns = 2 μs. The time step of the simulation was 2 fs.

We defined helical structure in terms of which regions of the Ramachandran map were occupied. The α_h region of the (ϕ, ψ) map was defined as $\phi \in [-100°, -30°]$ and $\psi \in [-67°, -7°]$. Residues which lay within the α_h region of the Ramachandran map were denoted as helical (h). All residues outside the α_h region were defined as "coil" (c). A helical segment was one which had at least three consecutive residues whose (ϕ, ψ) angles fall within the α_h boundaries (i.e., the smallest helix is …chhhc…). The fraction of helix for a given residue in the simulation was calculated as the fraction of time spent by that residue within helical segments.

3. Results and Discussion

To probe the structural integrity of the synthesized peptide-SWCNT complex, several binding affinity experiments were performed. First, using the method of surfactant-induced displacement (exchange), a relative measure of the hybrid's stability was determined. It is known that surfactant SDBS has a higher affinity for the surface of a SWCNT than short strands of DNA and thereby displaces the latter.[29] Surfactant exchange of the peptide, monitored through changes in NIR absorbance of the (6,5)-SWCNT, was attempted with SDBS as well as another surfactant, sodium cholate. Figures 1a,b, show that the effect of the two different surfactants on the peptide-SWCNT hybrid is slight at the elevated temperature of 60 °C over the course of 10 minutes. The effect of SDBS on the peptide-SWCNT sample is to broaden the peak with a significant appearance of a blue-shifted shoulder at 978 nm, characteristic of an SDBS-covered (6,5)-SWCNT, and an accompanying slight decrease of absorbance at 990 nm. Circular dichroism data (Supporting information, section S1) show little difference with or without the surfactant and whether or not the peptide is on the SWCNT or off it, suggesting that the peptide maintains its secondary structure through these exchange processes. Figures 1a and b should be compared to Figures 1c and d, which show the change in the NIR spectrum due to displacement by SDBS of the DNA sequence $(GT)_{30}$ or $(TAT)_4T$, respectively. These DNA sequences have been chosen for their, respectively, strong and weak binding affinities to the (6,5)-SWCNT.[29, 44] The $(GT)_{30}$ sample shows very little change over the course of the reaction; particularly absent is the blue-shifted shoulder at 978 nm. In contrast, $(TAT)_4T$ is almost immediately displaced from the SWCNT surface, evident in the blue-shifted peak. In addition, DNA-SWCNT surfactant exchange experiments show the existence of the (7,5)-SWCNT in the dispersion, with a starting absorbance peaking at 1040 nm (data not shown). This peak is absent in the peptide-SWCNT spectra, indicating the peptide's preferential ability to disperse the smaller-diameter

nanotube, (6,5). Strong and preferential binding of the peptide to the (6,5)-SWCNT, relative to DNA sequence $(TAT)_4T$, was confirmed by two-dimensional fluorescence maps of the 'ending' samples in Figure 1a and d (Figure S2 in Supporting Information).

Previous work on displacement of DNA molecules by SDBS from an SWCNT has shown that the process occurs by an initial fast step which was interpreted as conversion of SWCNTs with pre-existing defects to coating by SDBS.[29] This is followed by a slower second step with rate of displacement by SDBS limited presumably by the nucleation of defects. On this basis, we suggest that the emergent shoulder in Figure 1a represents displacement by SDBS of those hexacoiled peptides that have some form of defect. Over the time-frame of the experiment, it is clear that the remaining majority of SWCNTs in the sample strongly resist displacement by SDBS. By qualitatively comparing rates of SDBS exchange, we can rank the affinity of the examined biopolymers to the (6,5)-SWCNT as $(GT)_{30}$ > HexCoil-Ala > $(TAT)_4T$.

As another test of their binding affinities for the (6,5)-SWCNT, binary dispersions were created. The absorbance spectra for dispersions of $(GT)_{30}$, $(TAT)_4T$, or HexCoil-Ala mixed with SDBS and SWCNT are shown in Figure 1e. Observe that the HexCoil-Ala-SDBS-SWCNT absorbance spectrum has a peak at 992 nm but with a significant blue-shifted shoulder. Consistent with surfactant exchange data in Figure 1a, this suggests that two stable species exist in solution; surfactant-covered and peptide-covered SWCNT. By comparison, the $(GT)_{30}$ sequence out-competes SDBS for coverage of the SWCNT surface, as indicated by the fact that the absorbance peak remains centered at 992 nm. In contrast, the $(TAT)_4T$ sequence is out-competed by SDBS since the absorbance peak shifts to 980 nm. These experiments confirm that the relative binding strengths to the (6,5)-SWCNT can be ranked as $(GT)_{30}$ > HexCoil-Ala > $(TAT)_4T$.

The HexCoil-Ala-(6,5)-SWCNT hybrid structure has additionally been investigated by using REMD molecular simulation. (Further details can be found in the thesis of D. Roxbury.[45]) For the reported canonical form,[27] the hexacoiled structure overall remains stable during the REMD simulation, Figure 2a. The six strands, situated in anti-parallel configuration, remain adsorbed to the surface of the SWCNT in alpha-helical arrangements. Figure 2b shows the fraction of time that each residue is in a helical state. Except near the ends of the alpha helix, the six strand configuration in large measure retains its helicity over the course of the simulation. Residues near the ends of the alpha helix exhibit a certain degree of disorder as shown by a drop in fraction helix. On a long SWCNT with multiple strands along the nanotube length, this loss of structure will likely be quenched by additional hexacoiled structures placed on either side of the one in question. Convergence data can be found in supporting information, section S3.

The homohexamer HexCoil-Ala shows inhomogeneous patterns of helix-helix association upon binding to SWCNT. In the simulations, the overall configurations show little geometric variability for the hexamer (Figure S4a) after the initial equilibration step. There were two types of interfaces designed for HexCoil-Ala: leucine zipper and Ala-Coil (Figure S5). The former is a well-studied structural motif in proteins, while the latter is a tight antiparallel coiled-coil motif[46] that is common in transmembrane proteins.[47] The leucine zipper interface is formed along the interfaces between Chains B+C, D+E and F+G, and the Ala-Coil interface by Chains C+D, E+F and G+B (Figure 3a). The Ala-Coil interface displays much greater structural variability among different chains in its interhelical distance (Figure 3c, 3d). The leucine zipper interface has a trimodal distribution in interhelical distances among the chain pairs (Figure 3c), ranging from 9.5 to 11.0 Å. These values are well within the range seen for typical antiparallel helix dimers with Leu residues at similar positions in the sequence.[48]

The plasticity of the Ala-Coil interface causes large deviations from the designed model. In the tetrameric HexCoil-Ala crystal structure solved in the absence of SWCNTs (PDB ID: 3S0R), the Ala-Coil interface adopts an interhelical distance as small as 8.55 Å, quite similar to that intended in the original model of the hexamer. In the hexamer model designed to wrap SWCNT, the distance is 8.67 Å, but in the simulations, the average distance increases quite substantially to 13.0 Å, 13.0 Å and 9.86 Å, for Chains C+D, E+F and G+B, respectively. In contrast to the crystal structure and the original design of the hexamer, the alanine residues form much fewer interchain contacts in the simulations (Figures 3 a&b). In comparison, the configuration of the Leu-Zipper interface is robust. The interhelical distance in the tetramer crystal structure and the hexamer model is 10.5 Å and 10.6 Å, respectively. The average distance of Chains B+C, D+E and F+G is 10.3 Å, 11.2 Å and 10.4 Å, respectively. Interestingly, the great interhelical distance of the Ala-Coil interface extrudes Chain F from SWCNT (Figure 3a), causing helices E, F, and G to form three fourths of the classical four-helix bundle geometry. Thus the local arrangement of Chains E, F and G is reminiscent of the tetramer crystal structure (Figure S4b).

There is a single aromatic tyrosine residue in each monomer of the homohexamer. Originally, the Tyr residue was included as a spectroscopic label, and positioned at the helixhelix interface of the Ala-Coil directed outward towards solvent. However, the strong affinity of aryl groups for SWCNTs becomes apparent in the simulations, and might contribute to the deviation from the original, highly symmetric bundle geometry. There are three main clusters in the space of the distance from the phenyl ring atoms on the Tyr residue to SWCNT and the interhelical distance (Figure 3d). In Chains C+D, phenol groups always contact the SWCNT. Chains E+F and G+B both have two configurations: one phenol group is pointing inward and the other is tipping outside, and both of them are directed outward. However, Chains E+F occupy two separate main clusters with distinct interhelical distances, while Chains G+B have a continuous distribution of interhelical distance. The effect is to introduce a wider gap between the helices when the Tyr residues are able to penetrate into direct contact with the SWCNT. Thus the three chain pairs have distinct configurations for helix-helix interaction both in the leucine zipper and Ala-Coil interfaces.

Based on this analysis we can now speculate on the deviation of the observed structure from the design. The leucine zipper motif is greatly stabilized in water by the interdigitation of large apolar Leu side chains. By contrast, the smaller hydrophobic driving force for burial of the Ala residues at the Ala-coil interface makes this structure less stable. Indeed, the Ala-Coil is less frequently observed than the antiparallel leucine zipper in the crystal structures of water soluble proteins.[49] The lower stability of the Ala-Coil motif might provide greater malleability, and allow penetration of the phenol side chain of Tyr to the SWCNT. Clearly, this is a possibility that should be addressed in future designs.

4. Conclusions

We have examined the stability of de novo designed HexCoil-Ala-SWCNT hybrids by means of a surfactant-induced displacement reaction and by dispersion efficiencies in binary mixtures. These methods of ranking can be translated to a variety of non-covalent CNTwrapping polymers and small molecules. We find that the peptide binds stronger to the (6,5)-SWCNT than DNA sequence $(TAT)_4T$, but weaker than sequence $(GT)_{30}$. Results of REMD molecular simulation suggest that the proposed hexacoiled structure maintains its overall stability. The analysis of the hexamer configurations sheds light on the structure of the existing peptide and provides insights for the future design of more specific structures.

Supplementary Material

Refer to Web version on PubMed Central for supplementary material.

Acknowledgments

This work was supported by the National Science Foundation through grant CMMI-1014960, and a Faculty Innovation Grant (FIG) to AJ from Lehigh University. This research was also supported in part by the National Science Foundation through XSEDE resources under grants number [TG-MCB100049, TG-MCB120014]. WFD acknowledges support from NIH grant R37GM054616 and support from the MRSEC program of NSF to University of Pennsylvania.

References

1. Sementsov, Y.; Prikhod'ko, G.; Kartel, M.; Tsebrenko, M.; Aleksyeyeva, T.; Ulyanchychi, N. Carbon Nanotubes Filled Composite Materials: Carbon Nanomaterials in Clean Energy Hydrogen Systems - II. Zaginaichenko, SY.; Schur, DV.; Skorokhod, VV.; Veziroglu, A.; Đbrahimoğlu, B., editors. Vol. Vol. 2. Netherlands: Springer; 2011. p. 183-195.
2. Aikawa S, Xiang R, Einarsson E, Chiashi S, Shiomi J, Nishikawa E, Maruyama S. Facile fabrication of all-SWNT field-effect transistors. Nano Research. 2011; 4(6):580–588.
3. Nougaret L, Happy H, Dambrine G, Derycke V, Bourgoin JP, Green AA, Hersam MC. 80 GHz field-effect transistors produced using high purity semiconducting single-walled carbon nanotubes. Appl. Phys. Lett. 2009; 94(24) 243505-3.
4. Jin H, Heller DA, Strano MS. Single-particle tracking of endocytosis and exocytosis of single-walled carbon nanotubes in NIH-3T3 cells. Nano Lett. 2008; 8(6):1577–1585. [PubMed: 18491944]
5. Liu Z, Li X, Tabakman SM, Jiang K, Fan S, Dai H. Multiplexed multicolor raman imaging of live cells with isotopically modified single walled carbon nanotubes. J. Am. Chem. Soc. 2008; 130(41): 13540–13541. [PubMed: 18803379]
6. Welsher K, Liu Z, Daranciang D, Dai H. Selective probing and imaging of cells with single walled carbon nanotubes as near-infrared fluorescenct molecules. Nano Lett. 2008; 8(2):586–590. [PubMed: 18197719]
7. Zavaleta C, Zerda A, Keren S, Cheng Z, Schipper M, Chen X, Dai H, Gambhir SS. Noninvasive Raman spectroscopy in living mice for evaluation of tumor targeting with carbon nanotubes. Nano Lett. 2008; 8(9):2800–2805. [PubMed: 18683988]
8. Zerda A, Zavaleta C, Keren S, Vaithilingam S, Bodapati S, Liu Z, Levi J, Smith BR, Ma TJ, Oralkan O, Cheng Z, Chen X, Dai H, Khuri-Yakub BT, Gambhir SS. Carbon nanotubes as photoacoustic molecular imaging agents in living mice. Nat. Nanotech. 2008; 3:557–562.
9. Kostarelos K. The long and short of carbon nanotube toxicity. Nat. Biotech. 2008; 26:774–776.
10. Poland CA, Duffin R, Kinloch I, Maynard A, Wallace WAH, Seaton A, Stone V, Brown S, MacNee W, Donaldson K. Carbon nanotubes introduced into the abdominal cavity of mice show asbestos-like pathogenicity in a pilot. Nat. Nanotech. 2008; 3:423–428.
11. Liu Z, Cai W, He L, Nakayama N, Chem K, Sun X, Chen X, Dai H. In vivo biodistribution and highly efficient tumour targeting of carbon nanotubes in mice. Nat. Nanotech. 2007; 2:47–52.
12. Liu Z, Davis C, Cai W, He L, Chen X, Dai H. Circulation and long-term fate of functionalized, biocompatible single-walled carbon nanotubes in mice probed by Raman spectroscopy. PNAS. 2008; 105(5):1410–1415. [PubMed: 18230737]
13. Liu Z, Winters M, Holodniy M, Dai H. siRNA delivery into human t cells and primary cells with carbon nanotube transporters. Angew. Chem. 2007; 119:2069–2073.
14. Bahr JL, Mikkelsen ET, Bronikowski MJ, Smalley RE, Tour JM. Dissolution of small diameter single-wall carbon nanotubes in organic solvents? Chem. Commun. 2001:193–194.
15. Furtado CA, Kim UJ, Gutierrez HR, Pan L, Dickey EC, Eklund PC. Debundling and dissolution of single-walled carbon nanotubes in amide solvents. J. Am. Chem. Soc. 2004; 126:6095–6105. [PubMed: 15137775]

16. Huang X, Mclean SRL, Zheng M. High-Resolution Length Sorting and Purification of DNA-Wrapped Carbon Nanotubes by Size-Exclusion Chromatography. Anal.Chem. 2005; 77(19):6225–6228. [PubMed: 16194082]
17. Zheng M, Jagota A, Strano MS, Santos AP, Barone P, Chou SG, Diner BA, Dresselhaus MS, Mclean SRL, Onoa GB, Samsonidze GG, Semke ED, Usrey M, Walls DJ. Structure-Based Carbon Nanotube Sorting by Sequence-Dependent DNA Assembly. Science. 2003; 302(5650):1545–1548. [PubMed: 14645843]
18. Arnold MS, Stupp SI, Hersam MC. Enrichment of Single-Walled Carbon Nanotubes by Diameter in Density Gradients. Nano Lett. 2005; 5(4):713–718. [PubMed: 15826114]
19. Arnold MS, Green AA, Hulvat JF, Stupp SI, Hersam MC. Sorting carbon nanotubes by electronic structure using density differentiation. Nat. Nanotech. 2006; 1(1):60–65.
20. Bachilo SM, Strano MS, Kittrell C, Hauge RH, Smalle RE, Weisman RB. Structure-assigned optical spectra of single-walled carbon nanotubes. Science. 2002; 298:2361–2366. [PubMed: 12459549]
21. Dieckmann GR, Dalton AB, Johnson PA, Razal J, Chen J, Giordano GM, Munoz E, Musselman IH, Baughman RH, Draper RK. Controlled assembly of carbon nanotubes by designed amphiphilic peptide helices. J. Am. Chem. Soc. 2003; 125:1770–1777. [PubMed: 12580602]
22. Zheng M, Jagota A, Semke ED, Diner BA, Mclean SRL, Richardson RE, Tassi NG. DNA-assisted dispersion and separation of carbon nanotubes. Nat. Mat. 2003; 2:338–343.
23. Wang S, Humphreys ES, Chung S-Y, Delduco DF, Lustig SR, Wang H, Parker KN, Rizzo NW, Subramoney S, Chiang Y-M. Peptides with selective affinity for carbon nanotubes. Nat. Mat. 2003; 2(3):196–200.
24. Tu X, Manohar S, Jagota A, Zheng M. DNA sequence motifs for structure-specific recognition and separation of carbon nanotubes. Nature. 2009; 460(7252):250–253. [PubMed: 19587767]
25. Zorbas V, Ortiz-Acevedo A, Dalton AB, Yoshida MM, Dieckmann GR, Draper RK, Baughman RH, Jose-Yacaman M, Musselman IH. Preparation and Characterization of Individual Peptide-Wrapped Single-Walled Carbon Nanotubes. J. Am. Chem. Soc. 2004; 126(23):7222–7227. [PubMed: 15186159]
26. Hashida Y, Umeyama T, Mihara J, Imahori H, Tsujimoto M, Isoda S, Takano M, Hashida M. Development of a novel composite material with carbon nanotubes assisted by self-assembled peptides designed in conjunction with β-sheet formation. J. Pharm. Sci. 2012; 101(9):3398–3412. [PubMed: 22488097]
27. Grigoryan G, Kim YH, Acharya R, Axelrod K, Jain RM, Willis L, Drndic M, Kikkawa JM, DeGrado WF. Computational Design of Virus-Like Protein Assemblies on Carbon Nanotube Surfaces. Science. 2011; 332(6033):1071–1076. [PubMed: 21617073]
28. Zuo G, Xiu P, Zhou X, Zhou RH, Fang HP. Protein Conformational Changes Upon Binding with Carbon Nanotubes. Curr. Phys. Chem. 2012; 2(1):12–22.
29. Roxbury D, Tu X, Zheng M, Jagota A. Recognition ability of DNA for carbon nanotubes correlates with their binding affinity. Langmuir. 2011; 27(13):8282–8293. [PubMed: 21650196]
30. Roxbury D, Jagota A, Mittal J. Sequence-Specific Self-Stitching Motif of Short Single-Stranded DNA on a Single-Walled Carbon Nanotube. J. Am. Chem. Soc. 2011; 133(34):13545–13550. [PubMed: 21797248]
31. Roxbury D, Mittal J, Jagota A. Molecular-Basis of Single-Walled Carbon Nanotube Recognition by Single-Stranded DNA. Nano Lett. 2012; 12(3):1464–1469. [PubMed: 22375694]
32. Jorgensen WL, Chandrasekhar J, Madura JD, Impey RW, Klein ML. J. Chem. Phys. 1983; 79:926.
33. York DM, Darden TA, Pedersen LG. The effect of long-range electrostatic interactions in simulations of macromolecular crystals: a comparison of the Ewald and truncated list methods. J. Chem. Phys. 1993; 99(10)
34. Humphrey W, Dalke A, Schulten K. VMD - visual molecular dynamics. J. Molec. Graph. 1996; 14(1):33–38. [PubMed: 8744570]
35. Sugita Y, Kitao A, Okamoto Y. Multidimensional replica-exchange method for free-energy calculations. J. Chem. Phys. 2000; 113:6042–6051.
36. Sugita Y, Okamoto Y. Replica-exchange molecular dynamics method for protein folding. Chem. Phys. Lett. 1999; 314(1–2):141–151.

37. Johnson RR, Kohlmeyer A, Johnson ATC, Klein ML. Free Energy Landscape of a DNA-Carbon Nanotube Hybrid Using Replica Exchange Molecular Dynamics. Nano Lett. 2009; 9(2):537–541. [PubMed: 19161335]
38. Berendsen HJC, van der Spoel D, van Drunen R. GROMACS: a message-passing parallel molecular dynamics implementation. Comp. Phys. Commun. 1995; 91(1–3):43–56.
39. Lindahl E, Hess B, van der Spoel D. GROMACS 3.0: a package for molecular simulation and trajectory analysis. J. Mol. Model. 2001; 7(8):306–317.
40. van der Spoel D, Lindahl E, Hess B, Groenhof G, Mark AE, Berendsen HJC. GROMACS: fast, flexible, and free. J. Comput. Chem. 2005; 26(16):1701–1718. [PubMed: 16211538]
41. Best RB, Hummer G. Optimized Molecular Dynamics Force Fields Applied to the Helix–Coil Transition of Polypeptides. J. Phys. Chem. B. 2009; 113(26):9004–9015. [PubMed: 19514729]
42. Best RB, Mittal J. Balance between α and β Structures in Ab Initio Protein Folding. J. Phys. Chem. B. 2010; 114(26):8790–8798. [PubMed: 20536262]
43. Mittal J, Best RB. Tackling Force-Field Bias in Protein Folding Simulations: Folding of Villin HP35 and Pin WW Domains in Explicit Water. Biophys. J. 2010; 99(3):L26–L28. [PubMed: 20682244]
44. Khripin CY, Manohar S, Zheng M, Jagota A. Measurement of Electrostatic Properties of DNA-Carbon Nanotube Hybrids by Capillary Electrophoresis. J. Phys. Chem. C. 2009; 113(31):13616–13621.
45. Roxbury, D. Sequence Dependent Interactions Between DNA and Single-Walled Carbon Nanotubes. LEHIGH UNIVERSITY; 2012.
46. Gernert KM, Surles MC, Labean TH, Richardson JS, Richardson DC. The Alacoil: A very tight, antiparallel coiled-coil of helices. Prot. Sci. 1995; 4(11):2252–2260.
47. Walters RFS, DeGrado WF. Helix-packing motifs in membrane proteins. PNAS. 2006; 103(37): 13658–13663. [PubMed: 16954199]
48. Grigoryan G, DeGrado WF. Probing Designability via a Generalized Model of Helical Bundle Geometry. J. Mol. Bio. 2011; 405(4):1079–1100. [PubMed: 20932976]
49. Zhang S-Q, Kulp DW, Schramm CA, Senses A, DeGrado WF. A new dictionary of helix-helix interactions in membrane and solutble proteins. 2013 *(Under Revision)*.

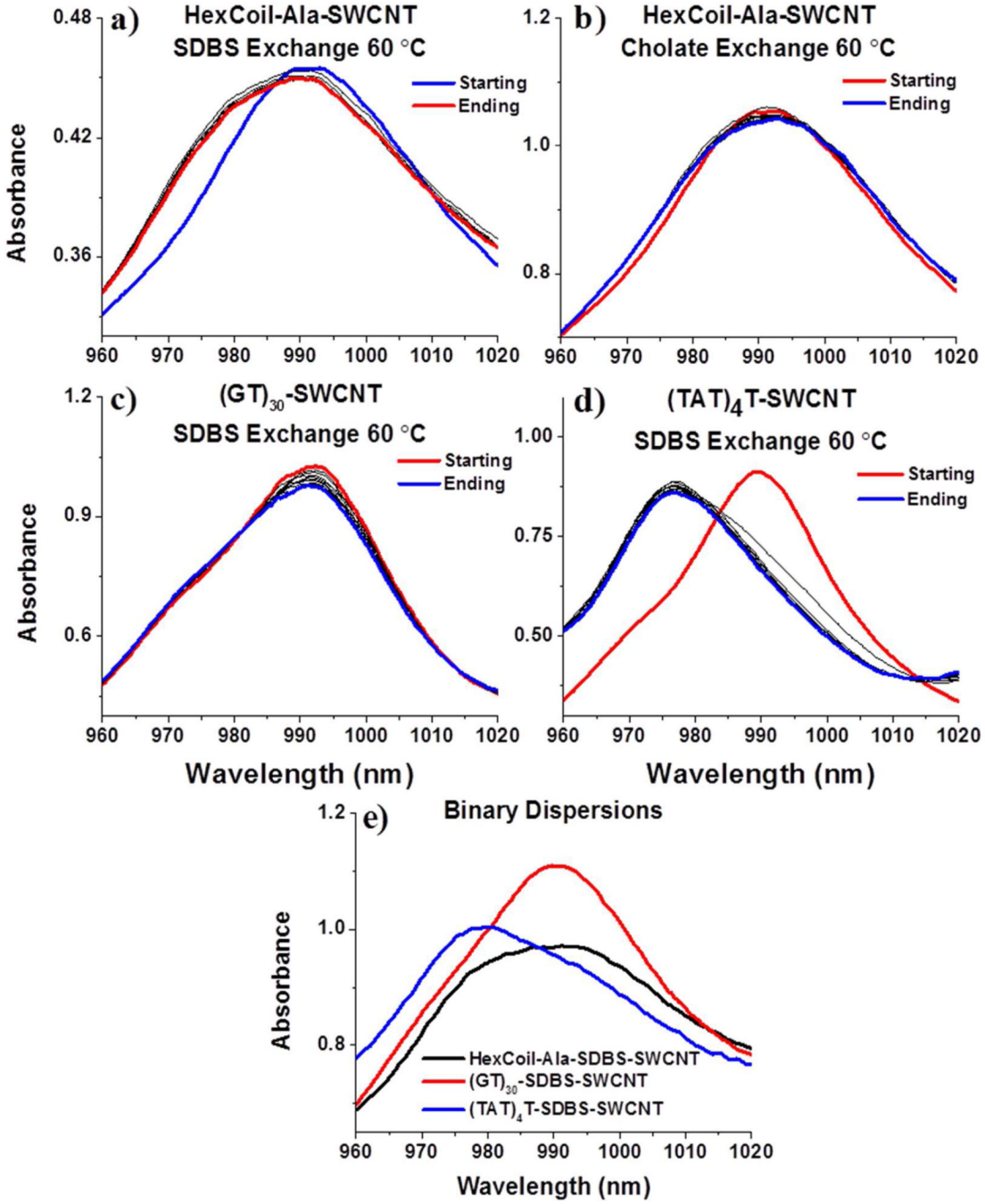

Figure 1.

Surfactant exchange performed on a HexCoil-Ala-SWCNT sample subjected to an excess of (a) SDBS and (b) sodium cholate at 60 °C for 10 minutes of incubation. For comparison, SDBS exchange is performed on samples of (c) $(GT)_{30}$-SWCNT or (d) $(TAT)_4$TSWCNT under the same conditions. (e) Binary dispersions of SDBS with $(GT)_{30}$, $(TAT)_4$T, or HexCoil-Ala. The peak position gives an indication of the relative binding strength of the biopolymer; a blue shift represents replacement by the surfactant molecule.

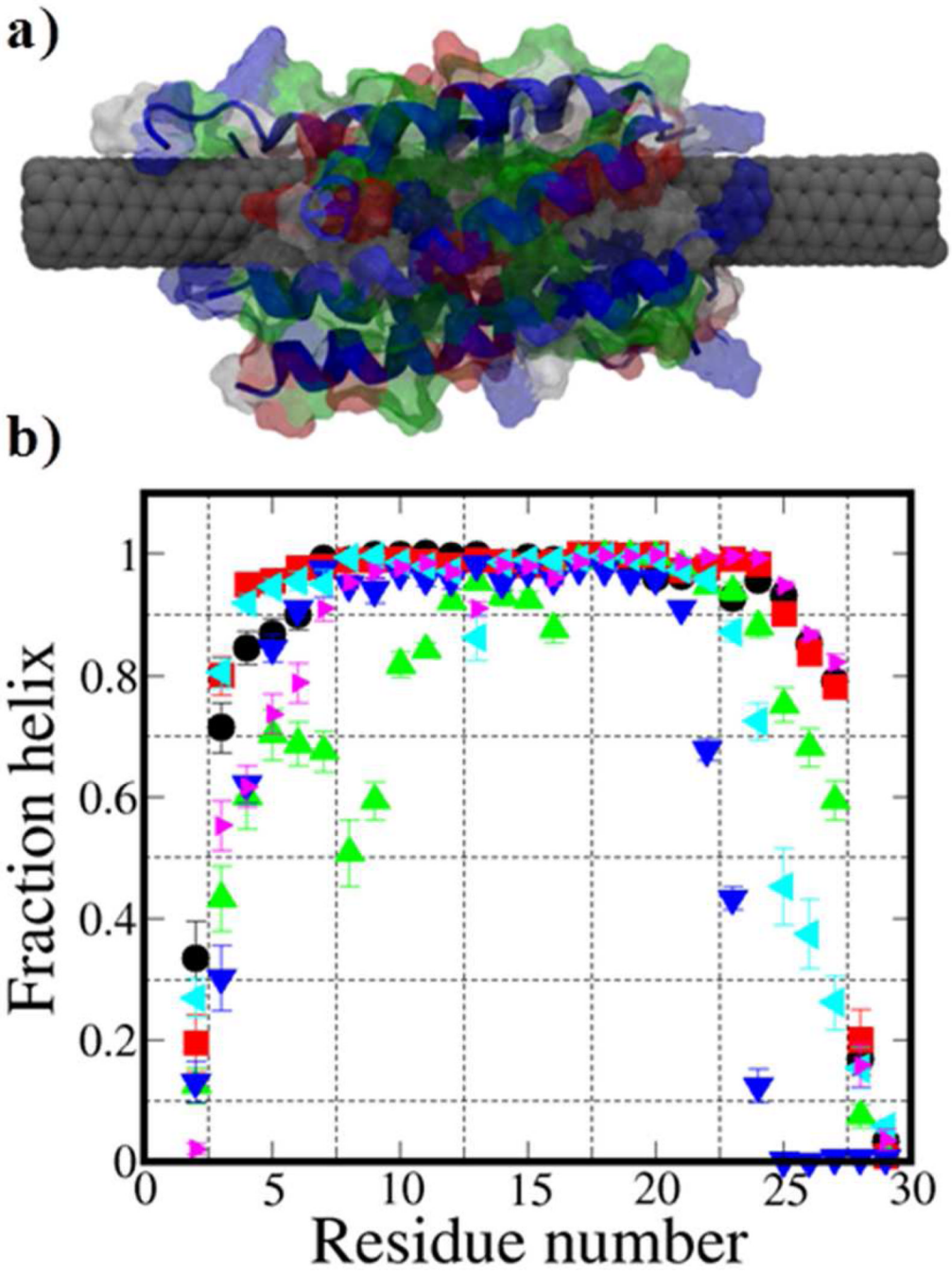

Figure 2.
(a) Equilibrium representations of the dominant structure for six strands of HexCoil-Ala peptide simulated on a (6,5)-SWCNT using REMD. (b) For each peptide (30 per strand), the fraction of the time spent in a helix is plotted.

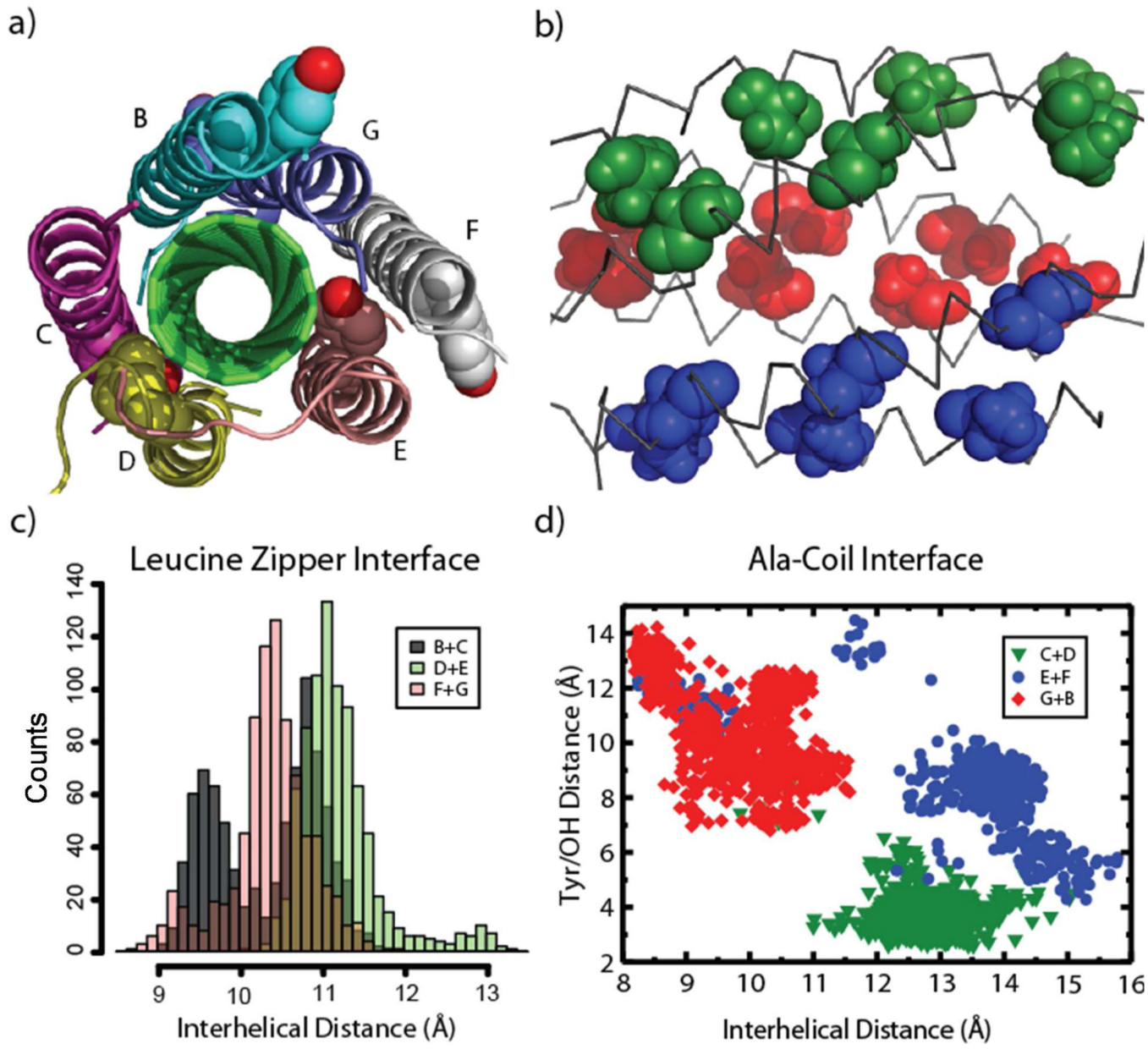

Figure 3.

(a) Side-on view of the hexamer with alanine residues shown in space-filling representation. Coloring scheme is the same as the legend in (d). (b) A representative equilibrium structure of the hexamer binding to SWCNT (green), looking down its axis. The chain names of the hexamer are labeled. The OH atom on the residue tyrosine is colored red. (c) Interhelical distance histograms of adjacent peptide dimers. (Colors additional to those in the legend represent overlapping parts of the distribution.) Here and for (d), the trajectory from 5 ns to 49.75 ns with an interval of 0.05 ns is used for calculation. (d) Distance of the hydroxyl group in tyrosine to SWCNT versus interhelical distance in Ala-coil pairs.